

Ferromagnetism and perfect spin filtering in transition-metal-doped graphyne nanoribbons

Jinbo Pan,¹ Shixuan Du,^{1,*} Yuyang Zhang,^{1,2,3} Lida Pan,^{1,2} Yanfang Zhang,¹ Hong-Jun Gao,¹ and Sokrates T. Pantelides^{2,3,†}

¹*Institute of Physics, Chinese Academy of Science, Beijing 100190, China*

²*Department of Physics and Astronomy, Vanderbilt University, Nashville, Tennessee 37235, USA*

³*Materials Science & Technology Division, Oak Ridge National Laboratory, Oak Ridge, Tennessee 37831, USA*

(Received 4 September 2014; revised manuscript received 2 November 2015; published 25 November 2015)

Ferromagnetism in half-metallic two-dimensional materials can lead to unique spintronics applications. Here we report first-principles calculations that predict monolayer graphyne nanoribbons (GyNRs), an alternative to graphene, doped randomly with 3d-series transition metal atoms at medium-to-high concentrations (2%–5%) can be ferromagnetic (FM). Furthermore, Mn- and Co-doped GyNRs are half-metallic with 100% spin polarization at the Fermi level and can act as perfect spin filters. The high spin polarization of the current is preserved up to large bias voltages. This study provides a basis for the fabrication of GyNRs with ferromagnetism and spin-polarized electron transport properties.

DOI: [10.1103/PhysRevB.92.205429](https://doi.org/10.1103/PhysRevB.92.205429)

PACS number(s): 73.61.Ph, 72.25.Mk, 73.22.-f, 75.50.Dd

I. INTRODUCTION

Recently, two-dimensional (2D) materials such as graphene have attracted considerable attention due to their ultrasmall thickness combined with extraordinary electronic [1,2], mechanical [3,4], and chemical properties [5,6]. However, it is still a great challenge to control the physical properties of these 2D materials and their derivatives. Among many possible applications, such carbon-based materials can potentially play a role in spintronic devices utilizing electron spins as the information carrier for high-capacity storage and for quantum computers [7,8]. To enable applications to spintronic devices, technical issues such as efficient spin injection, transport, control, and detection need to be addressed [7].

Currently, carbon-based spintronics is an emerging field that is attracting considerable attention as new materials and devices are being reported [9–11]. Significant efforts are devoted to the search for materials combining the properties of half-metallicity, high Curie temperature, ease of synthesis, and ease of incorporation into integrated circuits. In 2006, Son *et al.* reported calculations showing that zigzag graphene nanoribbons are half-metallic when an external transverse electric field is applied along the lateral direction [12]. Later, researchers found that cutting graphene into specific shapes [13–15], or edge-functionalizing and substitutionally doping graphene nanoribbons could also induce electronic spin polarization [16,17]. However, these methods are hard to implement. Till now, magnetism in graphene is sometimes observed when defects are present, which is very hard to control [18,19].

Doping graphene with 3d TM atoms adsorbed on the surface has also been considered [20,21] as a way toward spintronics. However, TM atoms tend to aggregate into clusters [22]. Meanwhile, other two-dimensional spintronic materials such as phthalocyanine-based organometallic porous sheets and graphitic carbon nitride have been theoretically predicted. However, they have disadvantages of low Curie temperature or difficult synthesis [23,24]. Materials with

mixed sp - sp^2 bonding have generated considerable attention for more than 20 years. Graphyne, a two-dimensional carbon allotrope with the same symmetry as graphene, has acetylene linkages between its nearest-neighbor rings. Large molecular segments of graphyne and two-dimensional sheets of graphdiyne have been successfully synthesized [25–29]. Subsequent studies suggest that these materials have attractive electronic properties [29–35]. Pan *et al.* reported that graphyne nanoribbons are semiconductors with band gaps similar to silicon [31]. A key property of graphyne are the larger rings, compared with the six-member rings in graphene, making it possible to introduce atoms in the same plane as the defect-free carbon sheet. A dilute concentration of select TM atoms at interstitial positions in graphyne has been found to induce half-metallicity [34,35]. He *et al.* studied the geometric structures and electronic properties of one-dimensional TM nanowires on graphyne. They found that the TM nanowires are stable out-of-plane and exhibit long-range magnetic order [36]. On the other hand, no devices have been fabricated so far based on either graphyne or graphdiyne.

In this paper we use first-principles calculations to examine the structure, magnetic, and transport properties of GyNRs doped randomly with TM atoms at medium-to-high concentrations. We find that the TM atoms are stable at their random positions and do not cluster. Mn- and Co-doped GyNRs exhibit 100% electronic spin polarization. The ground states of Cr-, Mn-, Fe-, and Co-doped GyNRs are ferromagnetic (FM), while that of V-doped GyNR is antiferromagnetic (AFM). Taking Co-doped GyNR as an example, we found that the spin-polarization effect can induce spin-polarized electron transport. At doping concentrations of 2%–5%, Co-doped GyNRs show a perfect spin-filter effect. These theoretical results may be useful in designing future devices.

II. CALCULATION METHODS

The structural optimizations and electronic structure calculations are performed within density functional theory and the local density approximation (LDA) by using the spin-polarized version of the Vienna *ab initio* simulation package (VASP) [37,38]. The projector augmented wave method is employed [39,40]. The electronic wave functions are expanded

*sxdu@iphy.ac.cn

†pantelides@Vanderbilt.Edu

in plane waves with a kinetic energy cutoff of 400 eV. A vacuum layer of 15 Å is used in the direction perpendicular to the ribbon plane and between the neighboring ribbons. The k -points mesh used in the calculations is $7 \times 7 \times 1$ for graphyne, and $7 \times 1 \times 1$ for GyNRs, generated automatically with the origin at the Γ point. Other choices of k points are tested, and the energy difference is found to be less than 0.005 eV. The structures are relaxed until the residual force on each atom is smaller than 0.01 eV/Å. For the FM and AFM calculations, to avoid being trapped in a local minimum, different initial magnetic moments were tested. In the case of AFM calculation for Co, for example, initial magnetic moments for adjacent Co atoms were chosen from $(1\mu_B, -1\mu_B)$ to $(3\mu_B, -3\mu_B)$. The Hubbard U correction (LDA + U) was also employed to compare the results with and without the correlation energy of the localized $3d$ orbital of TM atoms [41]. The rotationally invariant LDA + U formalism proposed by Dudarev *et al.* was used. $U_{\text{eff}} = U - J$ was used instead of individual U and J values.

The electronic transmission coefficient of Co-doped GyNRs is calculated using density functional theory (DFT) plus the nonequilibrium Green's function (NEGF) method as implemented in the ATK software [42–44]. The geometric structures of all the devices are optimized using the VASP package [37,38]. Transport calculations for the very thin GyNRs were tested by using both gold electrodes attached to small GyNR segments and TM-doped GyNRs as electrodes. The results for transport at zero bias are essentially the same. For the wider GyNRs, such calculations were impractical so that we used TM-doped GyNRs as electrodes. The unit-cell length in the electrode is about 7.0 Å. Single ζ and polarization orbitals (SZP) are used. The Hamiltonian overlaps and electronic densities are evaluated in a real space grid defined with a plane wave cutoff of 150 Ry to achieve a balance between calculation efficiency and accuracy.

Transmission coefficients are calculated using standard Green's function methods [45,46]. The device consists of three parts: the left and right electrode and the central scattering region, which contains the TM-GyNRs and parts of the leads to accommodate the molecule-electrode coupling interactions. The retarded Green's function of the scattering region $G_C(E)$ is constructed by the Hamiltonian of the scattering region (H_C) and the self-energies of the two semi-infinite electrodes $\sum_{L,R}(E)$, $G_C(E) = [E - H_C - \Gamma_L(E) - \Gamma_R(E)]^{-1}$, where $\Gamma_L(E) = i[\sum_L(E) - \sum_L^\dagger(E)]$ and $\Gamma_R(E) = i[\sum_R(E) - \sum_R^\dagger(E)]$ are the contact broadening functions associated with the left and right electrodes, respectively. The transmission probabilities are calculated as $T(E) = \text{Tr}[\Gamma_L G_C \Gamma_R G_C^\dagger]$.

III. ELECTRONIC PROPERTIES

Figure 1(a) illustrates the structure of a two-dimensional graphyne sheet. Because of the miniaturization tendency of electronic devices in applications, we cut the two-dimensional material into small stripes such as GyNRs and study the properties of TM-atom-doped GyNRs in contrast to previous studies [34–36] that reported the geometric and electronic structures of TM-doped graphyne. In addition, whereas previ-

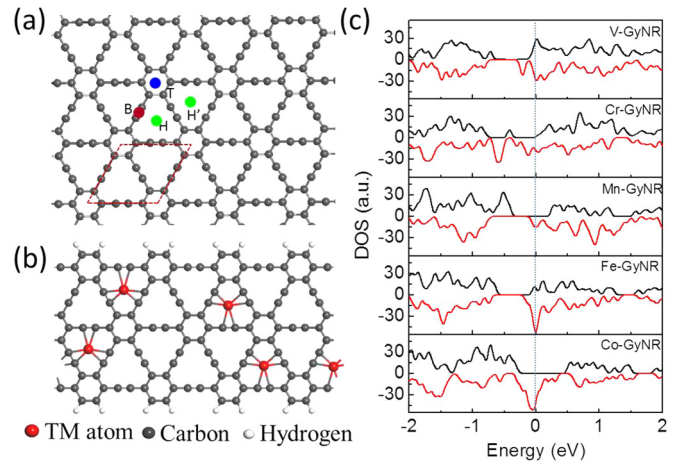


FIG. 1. (Color online) Configurations and DOS of graphyne and TM-atom-doped GyNRs. (a) Schematic of graphyne, the dashed rhombus indicates the primitive cell. The H, T, and B mark the possible doping sites we considered. H on the hollow site of the enlarged benzene ring, T on the top of the benzene ring, and B on the bridge site of a triple bond. (b) Structure of TM-doped GyNRs. (c) DOS of TM- (V, Cr, Mn, Fe, and Co) doped GyNRs, the black and red lines indicate the DOS for α and β spin. The energy of Fermi energy is set as zero.

ous works studied a dilute concentration of select TM atoms at interstitial positions in graphyne or strands of adjacent TM atoms that form nanowires, we investigated GyNRs doped randomly, though at large concentrations. The GyNRs are obtained by cutting through the graphyne sheet along the primitive cell vector.

All the TM atoms we studied (V, Cr, Mn, Fe, and Co) prefer doping GyNRs at the H site, similar to TM-doped 2D graphyne [35]. The binding energies per TM atom are calculated by $E_{\text{bind}} = (E_{\text{TM}} + E_{\text{GyNR}} - E_{\text{total}})/n$. Here the structure shown in Fig. 1(b) is defined as the supercell, E_{total} is the total energy of TM-GyNRs per supercell, E_{GyNR} and E_{TM} are the energies of isolated GyNR and TM atom, respectively, and n is the number of TM atoms. Their binding energies are 5.37, 4.03, 4.63, 5.94, and 6.45 eV, respectively. To elucidate the origin of such large binding energies, the total electron density around a Co atom and the six neighboring carbon atoms is shown in Fig. 2. It is clear that there is substantial orbital overlap between Co and carbon atoms, i.e., there is a strong covalent bond between Co and its surrounding carbon atoms. The reason for the strong interaction is that Co and the other TM atoms with partially occupied d orbitals are strongly active [47], which is different from the d^{10} element, e.g., Au, Ag, and Cu [48].

We tested the dimerization of two Co atoms on GyNRs. Various initial adsorption sites were tested for a Co dimer. After relaxation, the two Co atoms prefer to occupy different rings to maximize the Co-Co bonds. If the rings are adjacent, the energy is higher than if the two Co atoms are separated. We conclude that aggregation is not energetically favored and random doping prevails.

Considering that random doping is inevitable in experiments, we constructed randomly doped TM-GyNR structures as shown in Fig. 1(b). Their electronic properties including

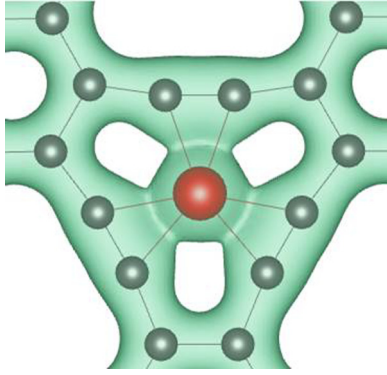


FIG. 2. (Color online) Charge density of Co and its surrounding carbon atoms. The isosurface value is $0.67 e/\text{\AA}^3$.

binding energies, spin polarizations, and magnetic moments are summarized in Fig. 1(c) and Table I. It can be seen that the binding energies per TM atom are very similar to those of a single TM atom per supercell, while larger than when two TMs are adjacent in a supercell. The smallest distance between two neighboring TM atoms in Fig. 1(b) is about 6.8\AA , larger than that in TM nanowire. It further suggests that TM atoms prefer network doping on GyNR rather than forming a TM nanowire.

The density of states of TM-GyNRs is shown in Fig. 1(c). Except for V-GyNR, all the other TM-GyNRs show spin-polarized density of states around E_f . The spin polarization is calculated by $SP = [(N_\alpha - N_\beta)/(N_\alpha + N_\beta)]_{E_f}$, where N_α and N_β are density of states for α and β spin at E_f , respectively. It is noteworthy that electron in Mn- and Co-doped GyNRs are 100% spin polarized at the Fermi energy, i.e., the GyNRs are half-metallic. The energy gaps of Mn- and Co-doped GyNRs for α spin are 0.8, and 0.97 eV, respectively. These numbers suggest a larger spin polarized range of Co-GyNR. In addition, Co-GyNR has a larger density of states for β spin at E_f compared to Mn-GyNR. These spin polarizations and also their magnetic moments can be elucidated by the projected density of states (PDOS) of TM atoms, as can be seen in Fig. 3. Considering a doped atom and its nearest surrounding molecular skeleton, TM-GyNR has an approximate D_{3h} symmetry similar with TM-doped graphyne. Therefore, the splitting modes of the d orbitals of the TM atoms in both GyNR and graphyne are 2-1-2 mode ($d_{xy}, d_{x^2-y^2}, d_{z^2}, d_{xz}, d_{yz}$) according to crystal field theory [35]. The $E2$ orbitals have the lowest energy, the $A1$ orbital comes second, and the $E1$ orbitals have the highest energy. In Co-GyNR, a Co atom has nine electrons in its outermost layer. Because of the spin

TABLE I. Spin-dependent energy gap (eV) and spin polarizability of TM-GyNRs.

TM	V	Cr	Mn	Fe	Co
E_{bind} (eV)	5.37	4.05	4.58	5.84	6.60
$E_G(\alpha)$ (eV)	0	0	0.8	0	0.97
$E_G(\beta)$ (eV)	0	0	0	0	0
SP	0	77.68%	100%	69.2%	100%
$M(\mu_B)$	0.61	2.0	3.0	1.88	1.0

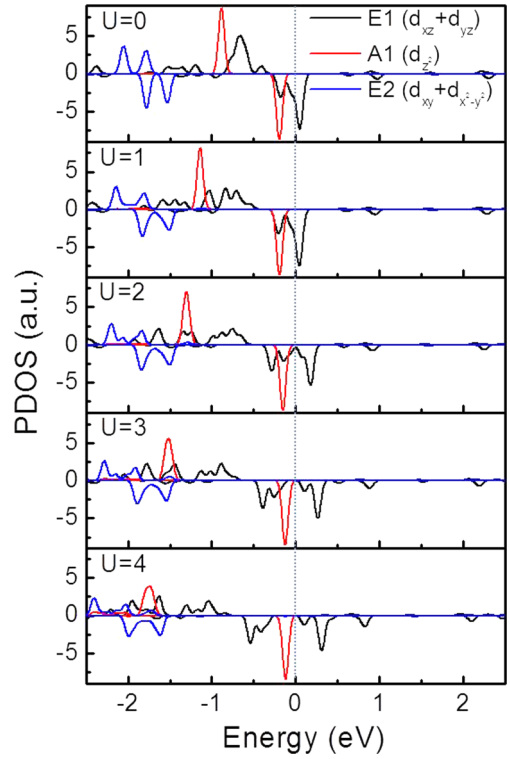


FIG. 3. (Color online) PDOS of Co-GyNR on single Co atom with different U . All the Co atoms have the similar PDOS. The PDOS above zero corresponding to α spin, while the PDOS below zero corresponding to β spin.

splitting, the electrons first occupy the lower energy orbitals. All five orbitals for α spin are occupied, while only four orbitals are occupied for β spin. The $E1$ orbitals for β spin are half-occupied, leading to spin-polarized density of states at E_f . The magnetic moment of Co-GyNR is thus $1\mu_B$ per atom.

We also employed the Hubbard U correction (LDA + U) to estimate the reliability of our results [41] because DFT may not describe the correlation energy of the localized $3d$ orbital of TM atoms correctly. The results are also shown in Fig. 3. It is found that the variation of U from 1 to 4 eV does not influence the results qualitatively. When $U = 0$, there is only one spin channel for both Co atoms around E_f . After employing a Hubbard U from 1 to 4 eV, the splitting of the $E1$ level increases a little, while the $A1$ and $E2$ levels almost do not change. Thus, the magnetic moment and spin polarization of Co-GyNR remain intact as the U changes. Because of electronic hybridization between V atoms and GyNR skeleton, the magnetic moment of each V atom in V-GyNR is about $0.6\mu_B$. The dependence of the binding energy of Co on U has also been tested. It varies from 6.6 to 5.1 eV as U increases from 0 to 4 eV.

IV. TRANSPORT PROPERTIES

According to previous papers [49,50] the transport properties of a molecular device depend closely on the spatial distribution of the frontier molecular orbitals. The presence of spin polarization does not guarantee a spin-polarized current. If the frontier molecular orbitals are highly localized, the

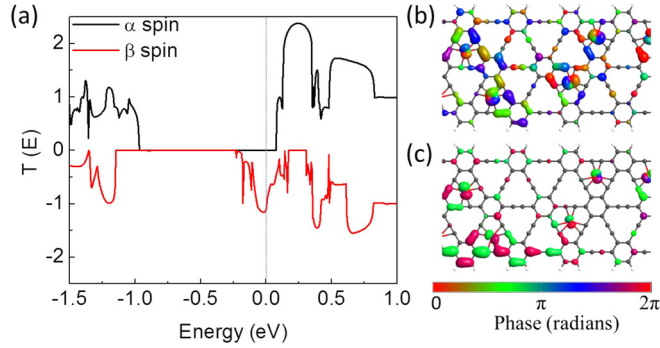


FIG. 4. (Color online) Transmission spectra of Co-GyNR (a) and its transmission eigenstate at Fermi energy (b) and (c) with different transmission eigenchannels. The isovalue is 0.3 a.u..

contribution to electron transmission may be small. We, therefore, calculated the spin-resolved transmission function $T(E)$ of Co-GyNR. Figure 4(a) shows the transmission function of Co-GyNR at zero bias. It can be seen that the transmission functions for electrons with α and β spin are clearly separated around the Fermi energy. The electronic transmission gaps around the Fermi energy for α spin are large, while the electronic transmission for the β spin exists around the Fermi energy, indicating a perfect spin filter effect. Figures 4(b) and 4(c) show the transmission eigenstates at the Fermi energy, the eigenstates located around the Co atoms, indicating that they are the key contributors to the spin-polarized transmission. Both transmission eigenstates originate from β spin with different transmission eigenchannels. The dependence of this result on the GyNR width could not be tested for wider GyNRs. Calculations on narrower GyNRs indicate that the half-metallic property and spin-polarized transport at the Fermi energy persist [51].

V. OTHER Co-doped GyNRs

Spin-polarized transport in Co-doped GyNRs depends on a stable FM state. Different doping concentrations and disorder of TM atoms on GyNRs could cause a variation of FM stability. In Fig. 5 we study the geometric and electronic properties of different randomly doped structures (structures I, II, III, and IV). Their exchange energies E_{ex} are calculated by

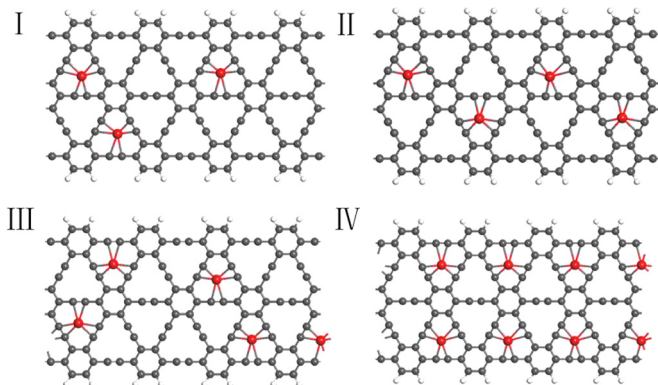


FIG. 5. (Color online) Configurations of different randomly doped Co-GyNRs.

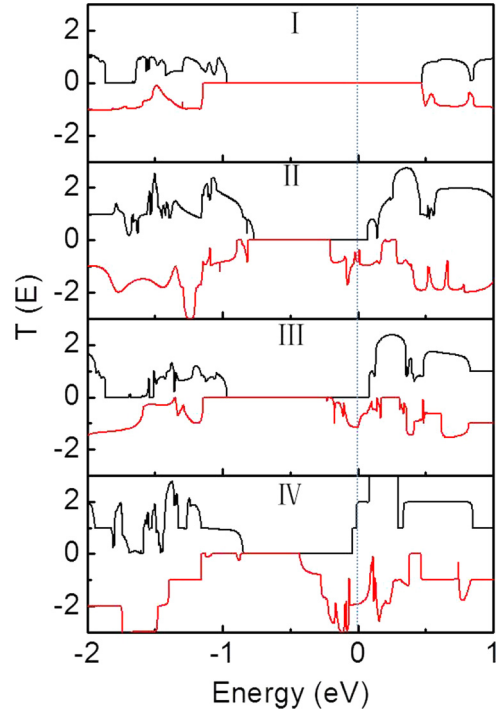


FIG. 6. (Color online) Transmission of different Co-GyNRs at zero voltage bias in Fig. 5.

$E_{ex} = (E_{AFM} - E_{FM})/n$ per unit cell, where E_{AFM} and E_{FM} are energies at AFM and FM states, and n is the number of Co atoms. It is interesting that all these random structures show FM ground states; their E_{ex} are 23, 17.5, 19.6, and 55.5 meV, respectively. The transmission coefficients of the TM-GyNRs at zero bias can be seen in Fig. 6. As suggested above, the Co atoms are the key contributors to the spin-polarized transmission around the Fermi energy. When the doping concentration of Co is very low, the distance between neighboring Co is large. It is very hard for electrons to tunnel among different Co atoms. The transmission of structure I at E_f is thus zero. When increasing the Co concentration, all the other Co-doped GyNRs show distinct spin-polarized transmission.

VI. MECHANISM FOR THE FM COUPLING

To elucidate the mechanism for the FM coupling, taking the structure in Fig. 5(I) as an example, we calculated the spin distribution and PDOS of two nearest-neighbor Co atoms and their surrounding carbon atoms. Independent whether the adjacent Co atoms are coupled in FM or AFM states, as shown in Figs. 7(a) and 7(b), the carbon atoms in the skeleton are strongly spin polarized due to the hybridization between the carbon orbitals and Co $3d$ orbitals. If the adjacent Co atoms are coupled in a FM state, the Co atoms and the carbon atoms form two spin arrangements $[\uparrow\downarrow\uparrow]$ and $[\uparrow\downarrow\downarrow\uparrow]$, as shown in Fig. 7(a). Such a magnetic coupling has been described by the superexchange mechanism, in which a spin-up polarization induces a spin-down polarization of its nearest neighboring atoms, forming the spin arrangement $[\uparrow\downarrow]_n$ [36,52]. If the adjacent Co atoms are coupled in an AFM state, the spin arrangements are $[\uparrow\downarrow\uparrow\downarrow]$ and $[\uparrow\uparrow\downarrow\uparrow\downarrow]$. But the total energy

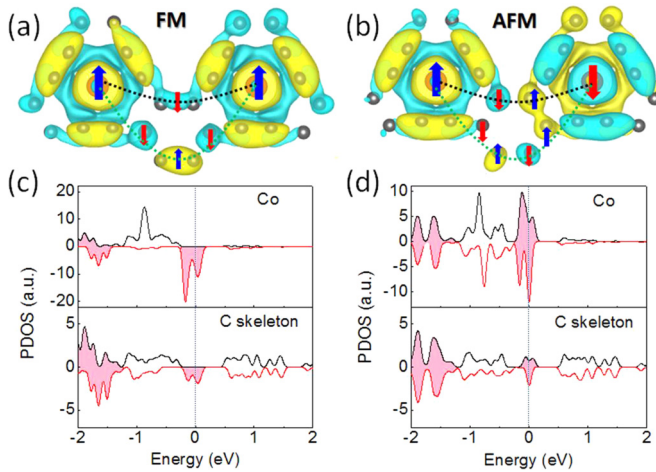


FIG. 7. (Color online) Spin distribution $[\rho(\alpha) - \rho(\beta)]$ (a) and (b) and PDOS of two nearest neighboring Co atoms ($3d$ orbitals) and their surrounding carbon atoms (c) and (d) of the structure in Fig. 5(I) at both FM and AFM states. The larger arrow indicates the spin of Co atoms, and the small arrow indicates the spin of carbon atoms. Yellow and green isosurfaces denote positive and negative values, respectively. The isosurface charge density is $0.002 e/\text{\AA}^3$.

of structures with an AFM spin order is higher than that at FM state. Although pristine graphyne is semiconducting, transition-metal-doped GyNRs are metallic, as demonstrated by the DOS plots in Fig. 7. Note that the states in the vicinity of the Fermi level, which arise from strong Co-C-Co interactions, have amplitude on both the Co atoms and the C skeleton.

VII. SUMMARY

In summary, we have systematically studied the electronic and magnetic properties of TM-doped GyNRs. We find that TM atoms prefer separately doping at the center of the enlarged benzene ring of GyNRs. The formed TM-GyNRs structure exhibits complete electronic spin polarization, similar to a two-dimensional sheet, and the d -orbital splitting pattern of TM atoms can be explained by crystal-field theory. Mn-GyNR and Co-GyNR have 100% electronic spin polarization. The calculation of electronic transmission further confirms that TM-doped graphyne and GyNRs can be applied in a spintronic device with 100% spin-polarized transmission at the Fermi level. The FM stability is also closely related to Co-doping concentration. The disorder of Co does not change the magnetic ordering of Co-doped GyNRs. The FM coupling of Co atoms is explained by a superexchange mechanism.

ACKNOWLEDGMENTS

The authors acknowledge financial support from the MOST (Grants No. 2011CB921702 and No. 2011CB808401), the NSFC (Grants No. 61390501, No. 51210003, and No. 51325204), and Collaborative Innovation Center of Quantum Matter of China. Supercomputer time was provided by National Supercomputer Center in Tianjin. Work at Vanderbilt is supported by the McMinn Endowment. Supercomputer time was provided by the National Center for Supercomputing Applications, and the Extreme Science and Engineering Discovery Environment (XSEDE), which is supported by National Science Foundation Grant No. ACI-1053575.

- [1] K. S. Novoselov, A. K. Geim, S. V. Morozov, D. Jiang, M. I. Katsnelson, I. V. Grigorieva, S. V. Dubonos, and A. A. Firsov, *Nature (London)* **438**, 197 (2005).
- [2] A. H. Castro Neto, N. M. R. Peres, K. S. Novoselov, and A. K. Geim, *Rev. Mod. Phys.* **81**, 109 (2009).
- [3] C. Lee, X. Wei, J. W. Kysar, and J. Hone, *Science* **321**, 385 (2008).
- [4] R. Grantab, V. B. Shenoy, and R. S. Ruoff, *Science* **330**, 946 (2010).
- [5] O. Leenaerts, B. Partoens, and F. M. Peeters, *Phys. Rev. B* **77**, 125416 (2008).
- [6] F. Schedin, A. K. Geim, S. V. Morozov, E. W. Hill, P. Blake, M. I. Katsnelson, and K. S. Novoselov, *Nat. Mater.* **6**, 652 (2007).
- [7] S. A. Wolf, D. D. Awschalom, R. A. Buhrman, J. M. Daughton, S. von Molnar, M. L. Roukes, A. Y. Chtchelkanova, and D. M. Treger, *Science* **294**, 1488 (2001).
- [8] A. R. Rocha, V. M. Garcia-Suarez, S. W. Bailey, C. J. Lambert, J. Ferrer, and S. Sanvito, *Nat. Mater.* **4**, 335 (2005).
- [9] N. Tombros, C. Jozsa, M. Popinciuc, H. T. Jonkman, and B. J. Van Wees, *Nature (London)* **448**, 571 (2007).
- [10] W. Han, K. Pi, K. M. McCreary, Y. Li, J. J. I. Wong, A. G. Swartz, and R. K. Kawakami, *Phys. Rev. Lett.* **105**, 167202 (2010).
- [11] W. Han, R. K. Kawakami, M. Gmitra, and J. Fabian, *Nat. Nano* **9**, 794 (2014).
- [12] Y. W. Son, M. L. Cohen, and S. G. Louie, *Nature (London)* **444**, 347 (2006).
- [13] O. Hod, V. Barone, and G. E. Scuseria, *Phys. Rev. B* **77**, 035411 (2008).
- [14] P. Potasz, A. D. Güçlü, A. Wójs, and P. Hawrylak, *Phys. Rev. B* **85**, 075431 (2012).
- [15] W. L. Wang, S. Meng, and E. Kaxiras, *Nano Lett.* **8**, 241 (2008).
- [16] F. Cervantes-Sodi, G. Csányi, S. Piscanec, and A. C. Ferrari, *Phys. Rev. B* **77**, 165427 (2008).
- [17] O. V. Yazyev and M. I. Katsnelson, *Phys. Rev. Lett.* **100**, 047209 (2008).
- [18] M. M. Ugeda, I. Brihuega, F. Guinea, and J. M. Gómez-Rodríguez, *Phys. Rev. Lett.* **104**, 096804 (2010).
- [19] Y. Wang, Y. Huang, Y. Song, X. Zhang, Y. Ma, J. Liang, and Y. Chen, *Nano Lett.* **9**, 220 (2008).
- [20] R. C. Longo, J. Carrete, and L. J. Gallego, *Phys. Rev. B* **83**, 235415 (2011).
- [21] K. T. Chan, H. Lee, and M. L. Cohen, *Phys. Rev. B* **83**, 035405 (2011).
- [22] R. Zan, U. Bangert, Q. Ramasse, and K. S. Novoselov, *Nano Lett.* **11**, 1087 (2011).
- [23] J. Zhou and Q. Sun, *J. Am. Chem. Soc.* **133**, 15113 (2011).
- [24] A. Du, S. Sanvito, and S. C. Smith, *Phys. Rev. Lett.* **108**, 197207 (2012).
- [25] R. Diercks, J. C. Armstrong, R. Boese, and K. P. C. Vollhardt, *Angew. Chem. Int. Ed. English* **25**, 268 (1986).

- [26] K. Kondo, S. Yasuda, T. Sakaguchi, and M. Miya, *J. Chem. Soc. Chem. Commun.* **1**, 55 (1995).
- [27] K. Tahara, T. Yoshimura, M. Ohno, M. Sonoda, and Y. Tobe, *Chem. Lett.* **36**, 838 (2007).
- [28] M. M. Haley, *Pure Appl. Chem.* **80**, 519 (2008).
- [29] G. Li, Y. Li, H. Liu, Y. Guo, Y. Li, and D. Zhu, *Chem. Commun.* **46**, 3256 (2010).
- [30] M. Q. Long, L. Tang, D. Wang, Y. L. Li, and Z. G. Shuai, *ACS Nano* **5**, 2593 (2011).
- [31] L. D. Pan, L. Z. Zhang, B. Q. Song, S. X. Du, and H. J. Gao, *Appl. Phys. Lett.* **98**, 173102 (2011).
- [32] D. Malko, C. Neiss, F. Viñes, and A. Görling, *Phys. Rev. Lett.* **108**, 086804 (2012).
- [33] J. J. Zheng, X. Zhao, Y. Zhao, and X. Gao, *Sci. Rep.* **3**, 1271 (2013).
- [34] J. He, S. Y. Ma, P. Zhou, C. X. Zhang, C. He, and L. Z. Sun, *J. Phys. Chem. C* **116**, 26313 (2012).
- [35] L. Pan, B. Song, J. Sun, L. Zhang, W. Hofer, S. Du, and H. J. Gao, *J. Phys. Condens. Matter* **25**, 505502 (2013).
- [36] J. He, P. Zhou, N. Jiao, S. Ma, K. Zhang, R. Wang, and L. Sun, *Sci. Rep.* **4**, 4014 (2014).
- [37] G. Kresse and J. Furthmüller, *Phys. Rev. B* **54**, 11169 (1996).
- [38] G. Kresse and J. Furthmüller, *Comput. Mater. Sci.* **6**, 15 (1996).
- [39] P. E. Blöchl, *Phys. Rev. B* **50**, 17953 (1994).
- [40] G. Kresse and D. Joubert, *Phys. Rev. B* **59**, 1758 (1999).
- [41] S. L. Dudarev, G. A. Botton, S. Y. Savrasov, C. J. Humphreys, and A. P. Sutton, *Phys. Rev. B* **57**, 1505 (1998).
- [42] J. M. Soler, E. Artacho, J. D. Gale, A. García, J. Junquera, P. Ordejón, and D. Sanchez-Portal, *J. Phys.: Condens. Matter* **14**, 2745 (2002).
- [43] M. Brandbyge, J.-L. Mozos, P. Ordejón, J. Taylor, and K. Stokbro, *Phys. Rev. B* **65**, 165401 (2002).
- [44] Atomistix ToolKit version 2014.1, QuantumWise A/S (www.quantumwise.com).
- [45] J. Taylor, H. Guo, and J. Wang, *Phys. Rev. B* **63**, 245407 (2001).
- [46] L. Zhang, J. Chen, and J. Wang, *Phys. Rev. B* **87**, 205401 (2013).
- [47] K. Nakada and A. Ishii, *DFT Calculation for Adatom Adsorption on Graphene* (INTECH Open Access Publisher, 2011), <http://www.intechopen.com/>.
- [48] M. Amft, S. Lebègue, O. Eriksson, and N. V. Skorodumova, *J. Phys. Condens. Matter* **23**, 395001 (2011).
- [49] J. Pan, Z. Zhang, X. Deng, M. Qiu, and C. Guo, *Appl. Phys. Lett.* **97**, 203104 (2010).
- [50] J. C. Ellenbogen and J. C. Love, *Proc. IEEE* **88**, 386 (2000).
- [51] See Supplemental Material at <http://link.aps.org/supplemental/10.1103/PhysRevB.92.205429> for configurations and transmission functions of Co-doped GyNRs with smaller width.
- [52] Y. Ma, Y. Dai, W. Wei, and B. Huang, *J. Mater. Chem. C* **1**, 941 (2013).